Synchronous Buck Converter based Low-Cost and High-Efficiency Sub-Module DMPPT PV System under Partial Shading Conditions

Hengyang Luo[a], Huiqing Wen[a,*], Xingshuo Li[a,b], Lin Jiang[b], Yihua Hu[b]

[a] *Department of Electrical and Electronic Engineering, Xian Jiaotong-Liverpool University, Suzhou 215123, China*
[b] *Department of Electrical Engineering and Electronics, University of Liverpool, Liverpool L69 3GJ, United Kingdom*

Abstract

The output power of long strings of photovoltaic (PV) modules are vulnerable to the effect of mismatching and partial shading among different level PV elements such as cells, sub-modules and modules. In this paper, a sub-module synchronous buck converter (SBC) with the distributed maximum power point tracking (DMPPT) control is presented in order to achieve optimal output power of the PV module, low system cost, and high efficiency even under partial shading conditions. Main shading patterns in a PV module are classified and their typical characteristics are illustrated. In order to improve the efficiency, a series-connected DC optimizer structure is implemented and a two-switch synchronous buck converter is delicately designed for each sub-module. A two-step perturb & observe based MPPT algorithm is adopted: firstly, a coarse tracking is implemented with large step size in order to improve the tracking speed and followed by a refined tracking process with a small step size with aim to minimizing the static oscillations. Furthermore, a bypass mode is triggered in order to maximize the system efficiency when no mismatch among sub-modules is detected. In the proposed sub-module DMPPT PV system, only the output voltage

*Corresponding author
Email addresses: Hengyang.Luo@xjtlu.edu.cn (Hengyang Luo), Huiqing.Wen@xjtlu.edu.cn (Huiqing Wen), Xingshuo.Li@xjtlu.edu.cn, X.Li31@liverpool.ac.uk (Xingshuo Li), L.Jiang@liverpool.ac.uk (Lin Jiang), Y.Hu35@liverpool.ac.uk (Yihua Hu)

is sampled, which reduces the current sensor and simplifies the implementation difficulty. A PV system with the proposed sub-module DMPPT algorithm and SBC power interface is bult in Matlab/Simulink. Main simulation results are provided for various shading patterns and working scenarios. A 100W low-cost and high efficiency sub-module integrated synchronous buck converter is designed and tested to show the effectiveness of the proposed DMPPT control by comparing the actual power yield under shading conditions.

Keywords: Photovoltaic (PV) system, distributed maximum power point tracking (DMPPT), synchronous buck converter (SBC), DC optimizer, partial shading, efficiency.

---

1. Introduction

As one of the most important sustainable energy sources, photovoltaic energy has been widely used in the last decade with the cost reduction of PV modules and government incentives [1]. Fig. 1 illustrates three different architectures for PV power systems, where both the voltage source inverter (VSI) [2] and the current source inverter (CSI) [3] can be used. However, considering the special efficiency requirements such as low-resistance and high-reverse-voltage devices, the CSI topology has not been widely used in industry [4]. In the conventional structure, as shown in Fig. 1(a), several PV modules are connected in series and a central DC-DC converter or DC-AC inverter is used as the power interface with the load or grid. Considering the nonlinearity of the PV modules with the irradiation and temperature variation, maximum power point tracking (MPPT) algorithms are necessarily used in order to ensure the PV modules operated in optimal states under any environmental condition[5]. These algorithms include: the perturb-and-observation (P&O) method [6], the incremental conductance method [7, 8], the fractional open circuit voltage method, the fuzzy logic control [9, 10], and neural network [11]. However, the effectiveness of these MPPT methods are obviously weakened under real-world partial shading or mismatch conditions [12], which are frequently happened due to various reasons: different

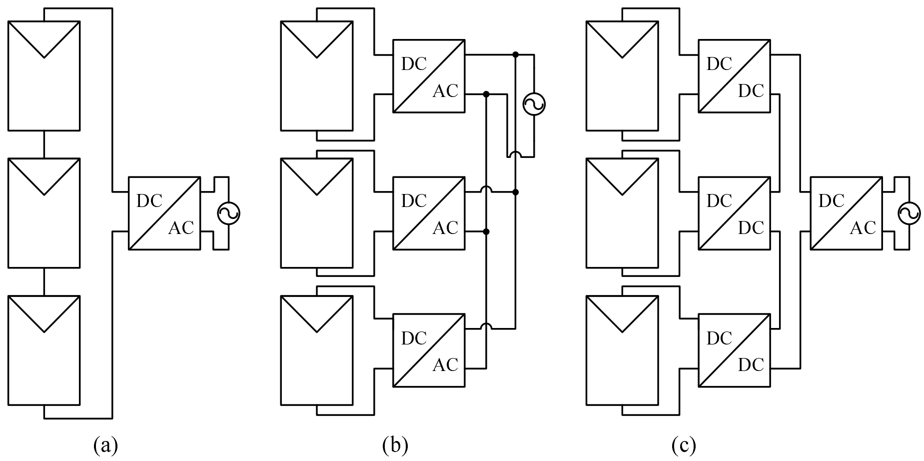

Fig. 1: Three PV system architectures: (a) Conventional structure; (b) Micro-inverter; (c) DC optimizer.

orientations, manufacturing tolerances, dirtiness, clouds, dust, and uneven aging among different level PV elements such as cells, sub-modules and modules [13]. The shaded PV elements operate at reverse-bias, consuming power similar as a resistive load instead of delivering power [14]. Partial shading will result in significant performance degradation especially for the center structure since the whole string current will be limited by the shaded cells or sub-modules with lowest current [15]. The whole PV string will even lose the total power for serious shading conditions [16].

To address the issues, many solutions have been proposed to achieve optimal output power [17]. Among them, anti-paralleled bypass diodes are commonly used in order to short circuit the shaded PV modules and reduce the power mismatching losses [18]. Although it can alleviate the mismatching effect partially, the available power of short-circuited PV modules is completely lost, furthermore, it will result in multi peaks in the P-V curve of the string [19]. Then, the conventional MPPT methods will be lost around the local peaks since they could not discriminate the local and global peaks [20]. To address this, global search algorithms such as colony optimization [21], particle swarm optimization [22], modified P&O [23], and the direct search method [24] must be used to locate the global peak position for partial shading conditions. However, the cost is greatly increased and the control becomes complicated. Besides, the shaded PV modules are short-circuited by the bypass diodes and this part power is totally unusable.

Distributed maximum power point tracking (DMPPT) techniques have been introduced by designing each PV module operated with individual maximum power point (MPP) [25]. Fig. 1(b) and (c) show two common DMPPT PV structures: the micro-inverter structure and the DC optimizer structure. In the micro-inverter structure, each PV module extracts its maximum output power without being affected by other modules [26]. Specifically, only the shaded PV sub-module is affected by the partial shading or mismatch conditions. It shows the advantages of modular design, power flexibility and simplicity. However, high voltage conversion ratio is required in this DMPPT PV structure since the output voltage level of each PV module is normally much lower than the utility voltage[27]. Thus, the overall power loss and system cost of micro inverter are high.

For the DMPPT based PV system, the system cost, efficiency and reliability issues related to DMPPT control are the major design challenges [28]. Fig. 1(c) shows the DC optimizer structure, where each PV module is regulated by its own dc-dc converter and a central inverter is used to exchange power with grid [29]. With this structure, each PV module can successfully operate under its MPP independently and the total power extracted the PV system is maximized. If the string output voltage can always stay within the optimal range, the MPP-T function in the central inverter is no longer required. Furthermore, since the input voltage of the central inverter is the sum of each PV module, a low conversion ratio design can be used, which is beneficial for the cost reduction and efficiency improvement [30]. Thus, a series-connected DMPPT PV system is implemented in this paper.

Typical topologies for the micro-converter include the Buck [31], Boost [32], Buck-Boost[33], SEPIC [34], and Zeta converter [35]. Among them, Buck converter is commonly used considering the positive output voltage polarity and less passive components. However, the power loss of the conventional Buck converter is high due to high conduction loss especially for low-power operating region. In this paper, a two-switch synchronous buck converter (SBC) is implemented in order to improve the efficiency. Furthermore, the SBC and DMPPT technique are dedicate for each PV sub-module instead each module in order to further improve the power yield, while previous research are mostly focused on the module-level micro-converter and DMPPT control [25, 28, 29, 30]. For each SBC, only the output voltage is sampled, which can remove the current sensor and greatly simplify the implementation difficulty. With the proposed design, both the system size and cost are reduced since low voltage devices with high switching frequency can be used in the SBC converter. Furthermore, both the static and dynamic tracking performance can be improved since a two-step perturb & observe based MPPT algorithm is adopted with a coarse tracking firstly implemented with large step size and followed by a refined tracking process with a small step size. When no mismatch is detected, a bypass mode is triggered in order to further maximize the system efficiency. The switching strategy of the SBC is designed to ensure smooth transition among different modes.

2. Shading Patterns Analysis

2.1. PV Module

The PV module (the SFP2136 monocrystalline silicon module produced by Singfosolar) is used and shown in Fig. 2. This PV module contains 9 blocks and each block includes 4 PV cells. Therefore, the PV module totaly includes 36 PV cells.

2.2. Shading Patterns

In a real environment, the shading conditions of a PV module can be divided into three patterns according to the position and severity of the shading. In the first pattern, the shading is uniformly distributed among all PV cells, such as the case of cells are shaded by cloud. For this kind of shading, the relationship of

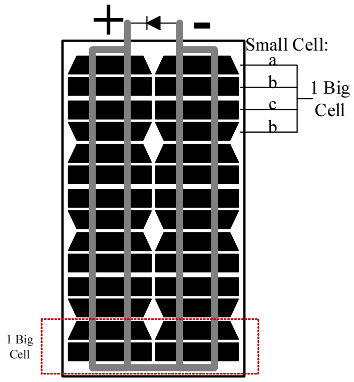

Fig. 2: PV module SFP3126.

the output power loss of the PV module with the reduction of the light intensity is close to linear. The other two patterns show uneven shading distribution: the shaded cells cannot generate current and they will consume power similar as a resistive load instead of delivering power, which is different from the first shading pattern. Fig. 3 shows the difference of the two shading patterns. Specifically, the pattern B indicates that several PV cells are partially covered by opaque objects such as mud and bird droppings, while the pattern C represents that one or several cells are completely covered by opaque objects.

(a) Shading Pattern A

Shading pattern A is illustrated in Fig. 3(a). The whole module, with all cells series connected, is covered by cloud. For this pattern, the light intensity is decreased due to the effect of the cloud compared with no shading condition . Typical characteristic curves of the PV string under this pattern is mainly determined by the light intensity. In Fig. 4(a), the I-V, P-V, P-I curves are illustrated. The output voltage is reduced slightly, while both the output current and power are reduced significantly.

(b) Shading Pattern B

Shading pattern B is illustrated in Fig. 3(b), where several cells are covered by opaque object and each of these cells is partially shaded. For this pattern,

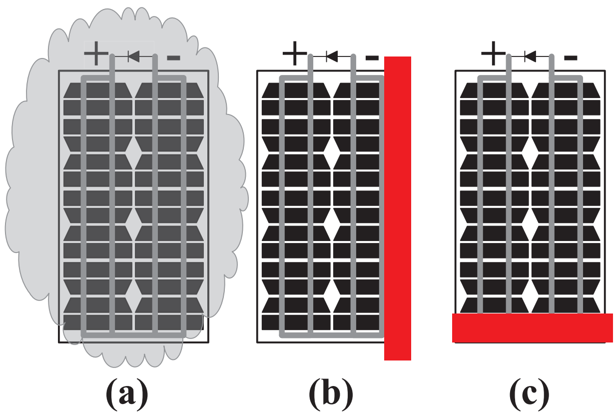

Fig. 3: Analysis of shading patterns: (a) Pattern A: all PV cells are covered by cloud; (b) Pattern B: several cells are partially covered ; (c) Pattern C: one or several cells are completely covered.

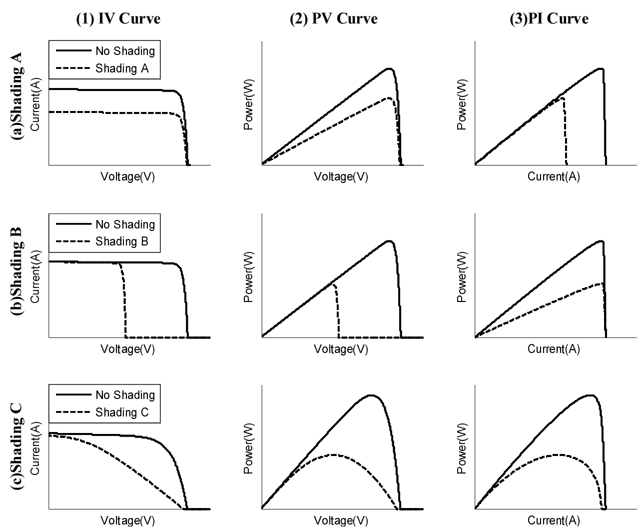

Fig. 4: Characteristic curves for different shading patterns including I-V Curves, P-V Curves, and P-I Curves.

the shaded cells still flow current of the whole module since the cells are series connected in the module or string. However, as illustrated in Fig. 4(b), the output voltage and power are decreased, while the output current keeps almost unchanged due to the shading effect.

(c) Shading Pattern C

Shading condition C is defined that the one or several cells are completely covered by opaque objects. As illustrated in Fig. 4(c), the maximum output voltage and current are reduces slightly,while the output power is reduced significantly.

2.3. Equivalent Circuit and Typical Curves

Considering the complexity of the pattern C, a detailed analysis with its equivalent circuit is presented here. Fig. 5 shows two scenarios for a PV module with n cells: no shading condition (a) and one cell is shaded (b).

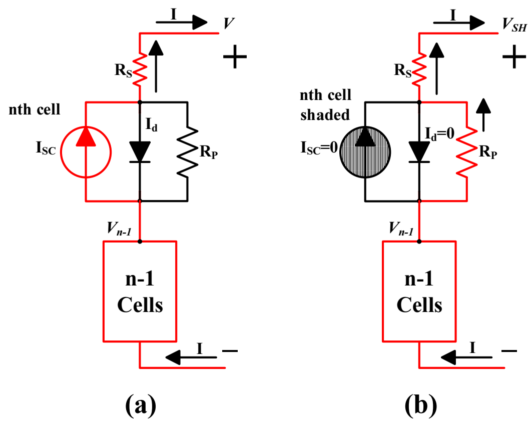

Fig. 5: Pattern C analysis with two scenarios: (a) no cells are shaded; (b) one cell such as the n_{th} cell is shaded.

In Fig. 5, one cell is represented by its equivalent electrical circuit while others are symbolled by a block with illustration its output voltage V_{n-1} and output current I. Fig. 5(a) shows that all PV cells are exposed in the high sunlight without any shading. The current in the n_{th} cell is equal to the string current since these cells are series connected. For this scenario, the n_{th} cell provides the same current as the string as other cells and each cell provides V/n output voltage. However, if one cell such as the n_{th} cell is completely shaded as shown in Fig. 5(b), the current provided by the shaded cell is zero. Thus, the string current flows through the parallel resistor R_P of the shaded cell. Since the diode is reverse biased, no current flows through the diode. The string current, provided by the other cells, must flow thought both the parallel resistor R_P and the series resistor R_S. The shaded cell acts a pure resistor in the whole string. Therefore, the output voltage is decreased for this scenario. For mathematic analysis, assume other cells still provides the same current as that no cell is shaded, thus, the output voltage is expressed by

$$V_{n-1} = (\frac{n-1}{n})V \tag{1}$$

The total output voltage of the whole string is expressed by

$$V_{SH} = V_{n-1} - I(R_P + R_S) = (\frac{n-1}{n})V - I(R_P + R_S) \tag{2}$$

The voltage drop caused by the shaded cell can be derived as:

$$\Delta V = V - V_{SH} = V - (\frac{1}{n-1})V + I(R_P + R_S) = \frac{V}{n} + I(R_P + R_S) \tag{3}$$

Compared with the parallel resistor R_P, the resistance of R_S can be ignored. Then, the expression of the voltage drop can be simplified as:

$$\Delta V \approx \frac{V}{n} + IR_P \tag{4}$$

Comparing with the output voltage under no shading condition, the actual output voltage for the same current is reduced since one cell is completely shaded in shading pattern C and the expression for the ΔV is shown above . Fig. 6 illustrates the comparison of the I-V curves of a PV string under two scenarios: without any shading and with one cell is completely shaded. The voltage drop due to one cell is shaded, ΔV, is also illustrated in this figure.

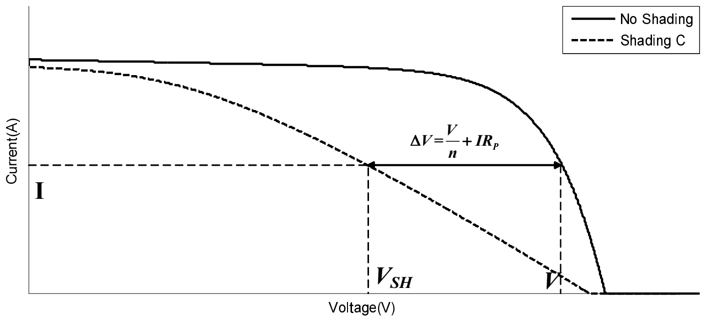

Fig. 6: Comparison of I-V curves for two scenarios: no cells shaded and with one cell completely shaded.

3. Sub-Module DMPPT Algorithm

As shown in Fig. 1(C), the output current of the DC optimizer is the same as the whole module current, which can be regarded as a constant for a specific environmental condition. Thus, the control algorithm of this DC optimizer based sub-module DMPPT PV system is implemented through two levels: (1) each DC optimizer is regulated to maximize its output voltage regardless of the whole module output voltage, and (2) the power conditioning system (PCS) of the central inverter is controlled to optimize the whole module output power. By simultaneously regulating through both two levels, the entire PV system can output its maximum power under any environmental condition. As discussed above, the synchronous buck converter (SBC) is used as the sub-module DC optimizer in order to reduce system cost and improve efficiency.

3.1. Two-Step MPPT Control

In order to increase the tracking efficiency and minimize the static oscillations, a two-step perturb & observe algorithm is implemented. As shown in Fig. 7, a coarse sweep step of the duty cycle is firstly implemented and the duty cycle range is set as 0.1 to 0.99. At the end of the first step, the duty cycle, corresponding to the quick-tracked point close to the actual maximum power point, is recorded for the second step: steady state maximum power point tracking process. In the second step, the duty cycle is perturbed with a small changing step to find a more accurate maximum power point. After the accurate maximum power point is tracked, the sub-module MPP tracker will continually oscillate around this point. Furthermore, the steady-state oscillations is greatly reduced since a smaller step size is used for the steady state.

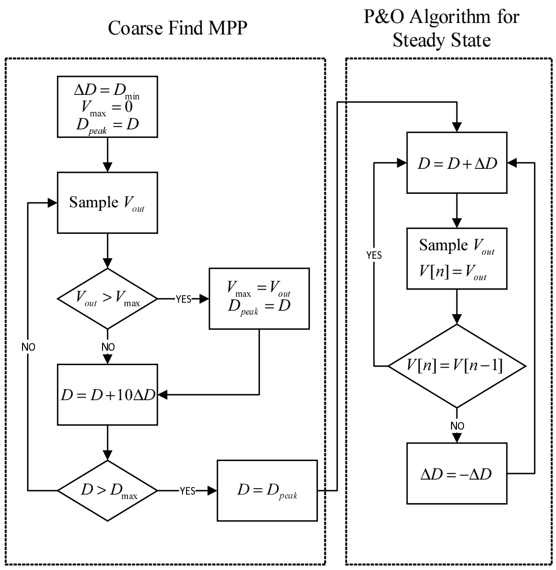

Fig. 7: Flowchart of the two-step P&O algorithm with only output voltage sampled.

3.2. Bypass Mode Control

The synchronous buck converter is operating with the two-step sub-module DMPPT tracking algorithm only when mismatch among the sub-modules is detected. However, once the mismatch conditions are disappeared, the synchronous buck converters need be short-circuited in order to maximize the system efficiency. Thus, a bypass mode is adopted in the central controller when mismatch conditions have not been detected.

Fig. 8 illustrates the operating modes for the bypass control The red parts represent the circuit actively connected in the system. Specifically, the SBC is active for the operating mode, as illustrated in Fig. 8(a). During the bypass mode, the bypass MOSFET is on and the SBC is deactivated.

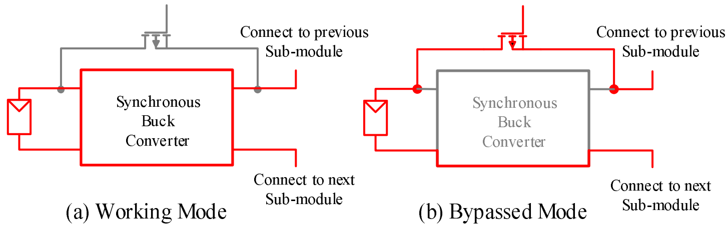

Fig. 8: Two modes illustration: (a) Operating mode for shading conditions; (b)Bypass mode.

Fig. 9 illustrates the flowchart for the bypass mode. The duty cycles of all sub-module SBCs are recorded by the central inverter controller. Since the S-BCs are connected in series and their output currents are equal, no mismatch among sub-modules indicates that all sub-modules are operating with the same output voltage, which is happened only when the duty cycles of SBCs are equal. Thus, once all duty cycles of the SBCs are measured equal, the bypass mode can be triggered. When the system is operating in the bypass mode, the mismatch can be detected by comparing the output voltages of the sub-modules. Once differences of the output voltages between SBCs are detected, the bypass devices are switched off and the two-step sub-module DMPPT algorithm for sub-modules is implemented.

4. Simulation

4.1. Shading Patterns Simulation

Fig. 10 shows the simulated curves of shading pattern A for different irradiations. The temperature is $25°C$. 6 curves are illustrated, representing different irradiations of $1000W/m^2$, $900W/m^2$, $800W/m^2$, $700W/m^2$, $600W/m^2$ and $400W/m^2$. For the shading pattern A, the only changing parameter is the light intensity, which is equivalent to the severity of the shading cloud. The simulation results show that the output power decreases with the irradiation.

Fig. 11(a) shows the simulated curves of shading pattern B. The same color is used for the same light intensity and the solid lines represent the curves without shading. The dashed lines represent the curves with equivalent one cell

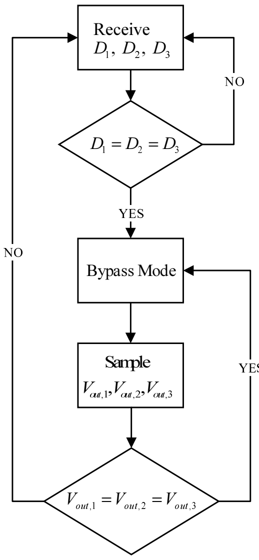

Fig. 9: Flowchart of the bypass mode.

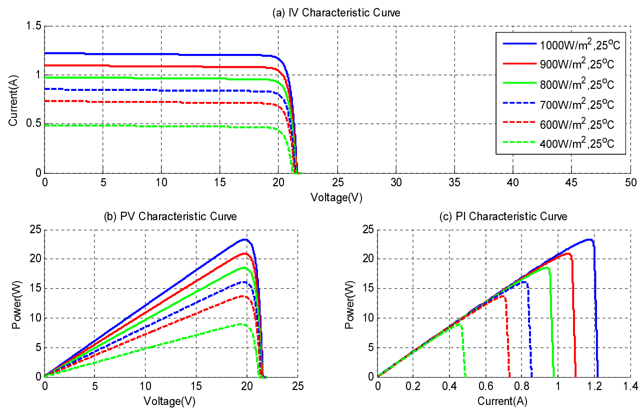

Fig. 10: Simulated curves for shading pattern A.

shaded. Compared with the curves with the same color, the output voltage for shading pattern B decreases while the output current keeps also unchanged under the same light intensity. Furthermore, if shading pattern B is considered, the changing tendency of the curves is similar.

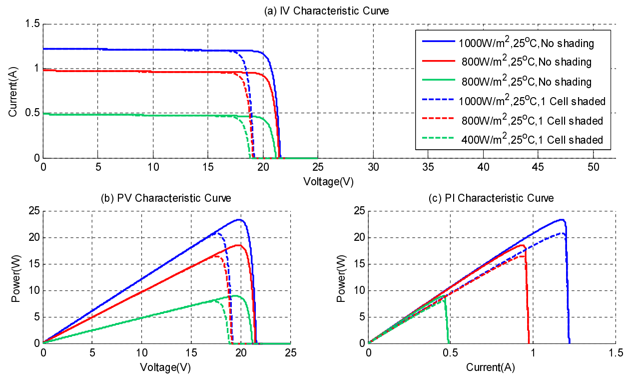

Fig. 11: Simulated curves for shading pattern B.

The simulated curves for the shading pattern C are shown in Fig. 12. Fig. 12(a) indicates that when one cell is completely shaded, both of the output current and voltage decrease.

The simulation results for different shading patterns indicates that the maximum power point of each sub-module will be changed no matter which kind of shading happens. For a PV module with series-connected sub-modules, if the shading is not uniformly distributed, mismatches will occur and the output power of the whole PV module will have multiple peaks. Thus, pattern B and C will result in mismatches between sub-modules and multiple peaks are occurred considering that the curve and shapes of the sub-modules are not the same.

4.2. Partial Shading Simulation without DMPPT Control

Fig. 13 shows the Simulink model of one PV module with two sub-modules series connected : PV_A and PV_B. The light intensity inputs for PV_A and PV_B are set as $800W/m^2$ and $400W/m^2$ respectively. The output current is set as 1.45A, which corresponds to the optimal output current of PV_A when it works

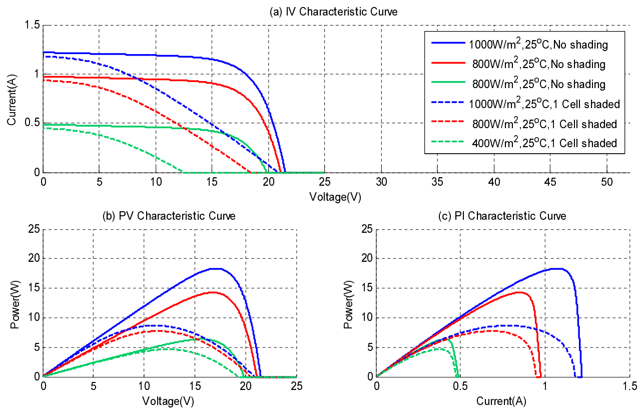

Fig. 12: Simulated curves for shading pattern C.

in MPP. The step size set for PV_A is 0.001%. For PV_B, since a two-step sub-module DMPPT algorithm is implemented, two step sizes are set with 3% for first-step tracking process and 0.02% for the second-step steady-state tracking.

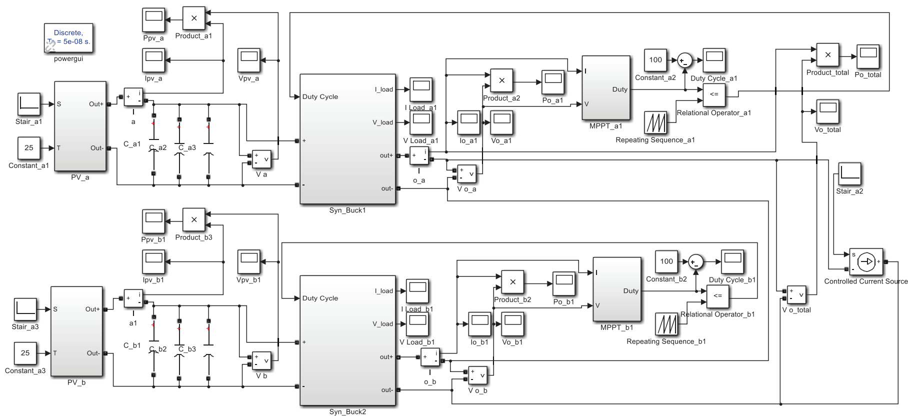

Fig. 13: Simulation model: two PV sub-modules series-connected.

Fig. 14 shows the simulation results with two PV sub-modules series-connected without DMPPT control. The green curve in Fig. 14(a) shows the output voltage of PV_A which is exposed to high light intensity. The red dotted line represents the output voltage of module PV_A when it works at its maximum power point. It shows that at the steady state, the simulated output voltage of the

PV_A is higher than the reference. The blue curve represents the voltage drop across the PV_B. The measured voltage across the PV_B is '-0.3V' since the PV_B is bypassed by the parallel connected diode whose turn-on voltage is set as 0.3. The zoomed part of the blue curve clearly indicates the voltage drop across the PV_B.

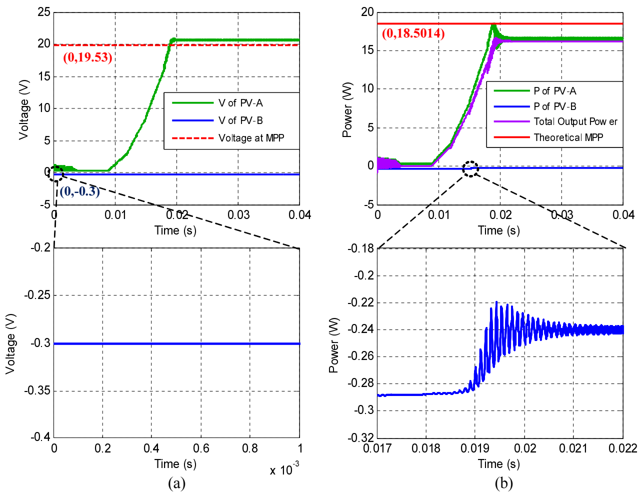

Fig. 14: Simulation result when two PV sub-modules are series-connected without DMPPT control.

Fig. 14(b) shows the simulation results of the output power. The green curve shows the output power change of PV_A. The purple line shows the total output power of the SBC. It shows that the purple is slightly lower than the green line. Sine the bypass diode of the PV_B is on, some part of power is consumed by the bypass diode, thus, the total output power is lower than the output power of PV_A. The red line shows the theoretical maximum output power the PV_A. It shows that the shaded sub-module PV_B not only has negative effect the series-connected PV module, but also limit the total output power. The blue line represents the power consumed by the PV_B. The zoomed part of the blue cure shows the consumed power of PV_B, which indicates a reduced input current of the synchronous buck converter.

Fig. 15 shows the simulated result of the converter input current. The red line shows the output current of the PV_A for $800W/m^2$. It shows that the output current for steady-state is lower than the output current of PV_A at MPP. Thus, with a shaded PV sub-module series connected, the working point of PV_A biases to right side of the maximum power point. With the same zoom ratio as the Fig. 15, the current changing details are illustrated. The current begins to decrease at $0.019s$, which is the same time when the power of PV_B begins to decrease.

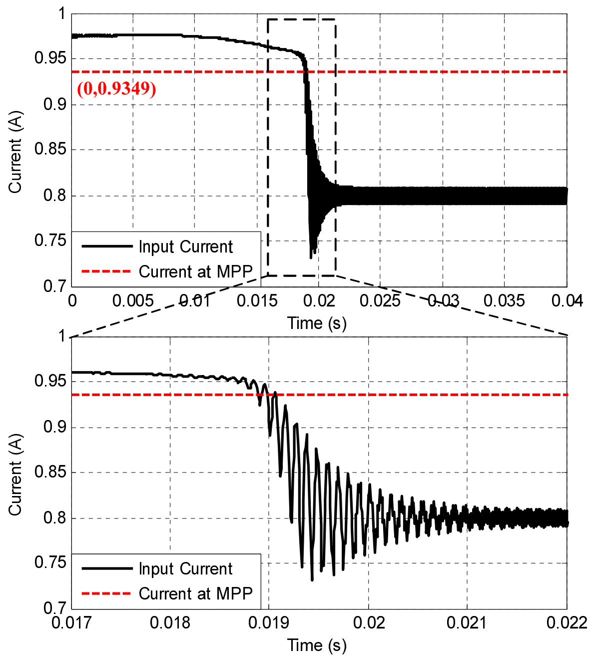

Fig. 15: Simulated input current of the sub-module SBC without DMPPT control.

4.3. Partial Shading Simulation with Sub-Module DMPPT Control

Fig. 16 shows the partial shading simulation results with the proposed SBC and sub-module DMPPT control. In Fig. 16(a), the green curve and the blue curve represent the output power of PV_A and PV_B respectively. The green dashed line shows the maximum power of the PV_A. This figure indicates that the sub-module PV_A is working at its MPP for the steady state, while the output power of the PV_B is lower than the theoretical maximum power at $400W/m^2$. Moreover, the tracking start time of the shaded sub-module is later than the unshaded sub-module.

If both of the two sub-modules work in their individual maximum power points, the maximum output power will be $27.424W$, as indicated by the red dashed line of Fig. 16(b). The red solid curve shows the total output power. As shown in Fig. 16, although the total output power is lower than the sum of the maximum powers when two sub-modules work at their MPPs, the proposed scheme can significantly improve the total output power.

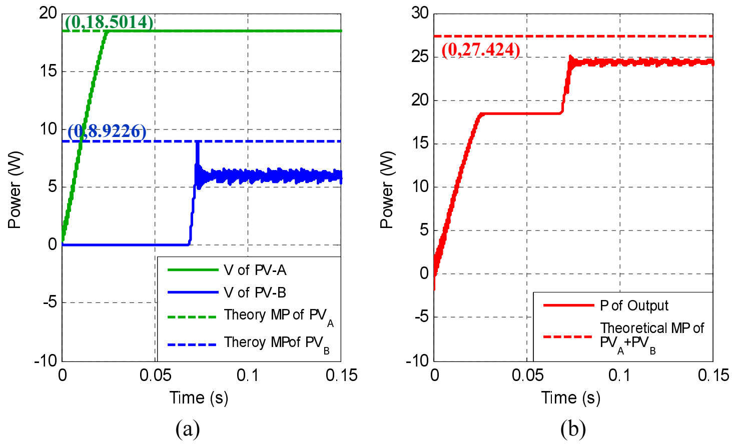

Fig. 16: Simulation results of the output powers.

4.4. Comparison and Discussion

Fig. 17 shows the effect of the proposed method on the total module output power. In Fig. 17(a), the purple curve shows the total module output power without the DMPPT control. In this module, two independent sub-modules are series connected. The red curve shows the total module output power with sub-module DMPPT control. Fig. 17(b) shows the zoomed output power for the steady state. The average output power with sub-module DMPPT control is $24.4W$, while the corresponding value without DMPPT control is $16.2W$. The efficiency improvement by applying sub-module DMPPT technique can calculated as 50.167%. Since only two sub-modules are analyzed in the simulation, the efficiency improvement for real PV plants will be more significant considering large number sub-modules or modules are series-connected.

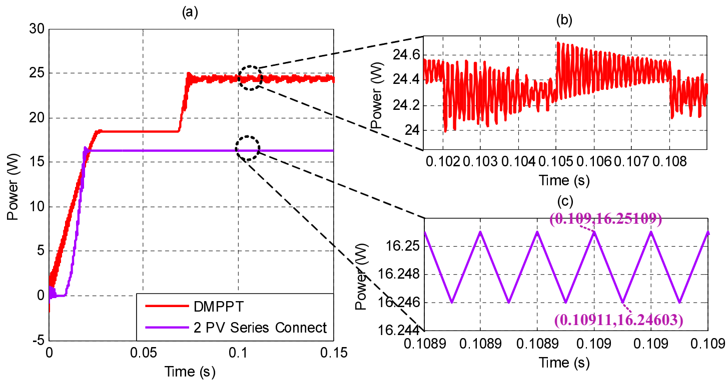

Fig. 17: Effects of the output power with the sub-module DMPPT algorithm.

Fig. 17 illustrates the comparison results with the simulated P-I curves. The blue curve shows the P-I curve of PV_A with $800W/m^2$ irradiation. The aquamarine blues curve indicates the P-I curve of PV_B with $400W/m^2$ irradiation. The maximum power points of these two PV sub-modules show distinct features. When the two PV sub-modules are series connected with no bypass didoes parallel-connected, the performance of the module output power will be significant limited by the mismatch, as shown by by the gray curve. The green curve shows the P-I curve with the bypass diodes parallel-connected. By comparing with the two curves, it can be seen the by bypass diode can effectively enhance the whole output power. The sum of PV_A and PV_B is shown by the pure line, which is overlapped with the purple. If the sub-module DMPPT is used, the performance of the whole system is improved,as indicated by the red curve. Furthermore, multiple maximum power peaks are eliminated. Both the range of the output current and power are enlarged. As illustrated in Fig. 17, the measured maximum output power is $25.028W$ when the output current is $0.9344A$. At this point, the synchronous buck converter, which is connecting with the PV_A is deactivated since the PV_A is working in its MPP. If the SBC is connected, the whole output will be limited. Since the buck converter can only boost the input current, the input side current will must less than the current at the MPP. Therefore, at this point, the buck converter should be not connected in the system, and the PV_A should supply power directly to the load. The green line indicates that the module output power for this scenario is $18.67W$. Then, the efficiency improvement by using sub-module DMPPT can be computed as 34.05%.

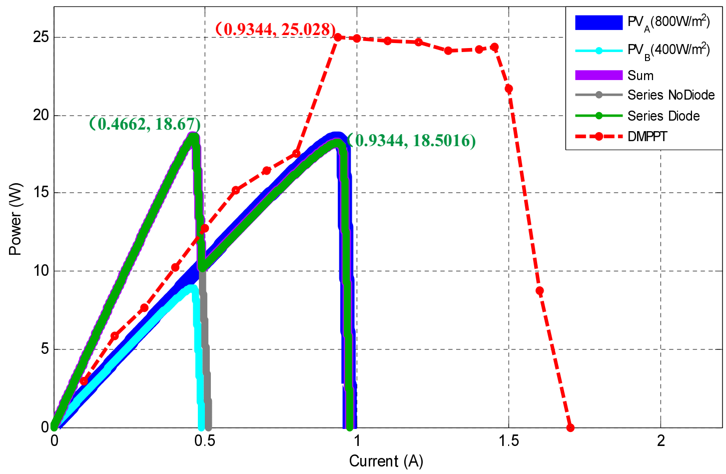

Fig. 18: Simulation comparison of P-I curves with various methods under shading conditions.

5. Experiments

5.1. Hardware Design

Considering different applications, two version of the synchronous buck converter are design: module level SBC with DMPPT control and sub-module level SBC with DMPPT control. Fig. 19 shows the photograph of the module level SBC hardware dedicated for PV modules that are series connected in a field PV plant.

In Fig. 20, the photograph of the low power version synchronous buck converter dedicated for one sub-module is presented. It shows that the SBC can

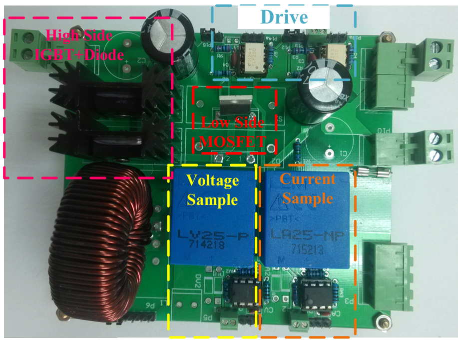

Fig. 19: Photograph of the module level SBC hardware.

be directly assembled with the junction box of a solar board. As shown in Fig. 20(b), the main part of the design prototype has the same size as the smallest Chinese coin, which the diameter is $19mm$.

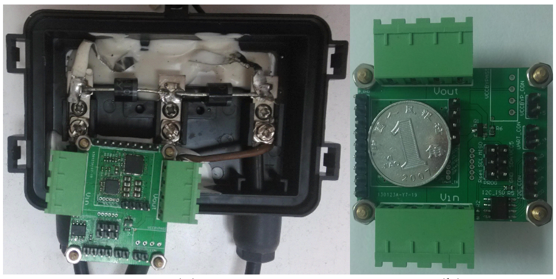

(a) (b)

Fig. 20: Photograph of the sub-module SBC hardware: (a) integration with the junction box of a PV module; (b) comparison with a Chinese coin.

The bill of main materials are list in the Table. 1, where ATtiny861 is the controller for the SBC. The input voltage of the converter is sensed with a low-poss filter and send to the main controller. Similar, the output voltage is measured as one input of the main controller. The difference of the measured voltage is just the the average voltage across the inductor of SBC. Then the current flows through the inductor is obtained. $FDMF6704A$ is a power integrated chip that combines two power MOSFETs, gate driver circuit, and a Schottky diode altogether. The size of $FDMF6704S$ is small, specifically,

$6mm \times 6mm$. Thus, the total area of the PCB is small and the system cost is also reduce. $ADUM1250$, which can transfer information bidirectionally, is used to monitor states of sub-modules, including the input voltage, output voltage, and duty cycle of SBCs. It can also communicate between the the sub-module SBCs and the cental controller. The bypass mode is controlled by MOSFET $AO3400$. During this mode, the SBC is short-circuited and the PV module directly connects with the central invert. Considering the power loss of the bypass MOSFET, the drain to source on-state resistance $R_{DS(on)}$ should be kept as low as possible. $AO3400$ is selected as the bypass MOSFET in the practical design since its $R_{DS(on)}$ is less than $33m\Omega$ when the gate voltage is $4.5V$. The efficiency can be further improved by replacing $AO3400$ with $SI4448DY$ since the $R_{DS(on)}$ of $SI4448DY$ is only $1.4m\Omega$.

Table 1: Main components and cost breakdown

Comment	Description	Quantity	Footprint	Cost(RMB)
PCB Board	Printed Board	1		5
FDMF6704A	DrMos	1	FDMF	12
ATTingy861	Microcontroller	1	32M1-A	18
SER1360-103KL	Inductor	1	L	9
B0505S/D-1W	DC-DC Isolator	1	SIP	4.5
AO3400	Bypass MOSFET	1	SOT23	0.3

5.2. PV Characteristics Test

In the experiments, the PV module SFP2136 is used and shown in Fig. 2 . Considering the manufacturing tolerances, the characteristics of total five modules from the same company are measured. The test procedure is described here: firstly, each PV module is directly connected with the adjustable electric load $IT8514$. In order to test the characteristic of the PV modules under various light intensity values, different lamps are used to emulate the natural sunlight. In the experiment, the lamps and the PV modules are fixed to the same position.

The output current is tuned from zero to a maximum value that corresponds to zero module output voltage. The step size of the output current is $0.01A$ considering the precision of the electric load. The output voltage and the output power can be directly measured from the electric load $IT8514$. An electrical fan is used to maintain the temperature of PV module constant.

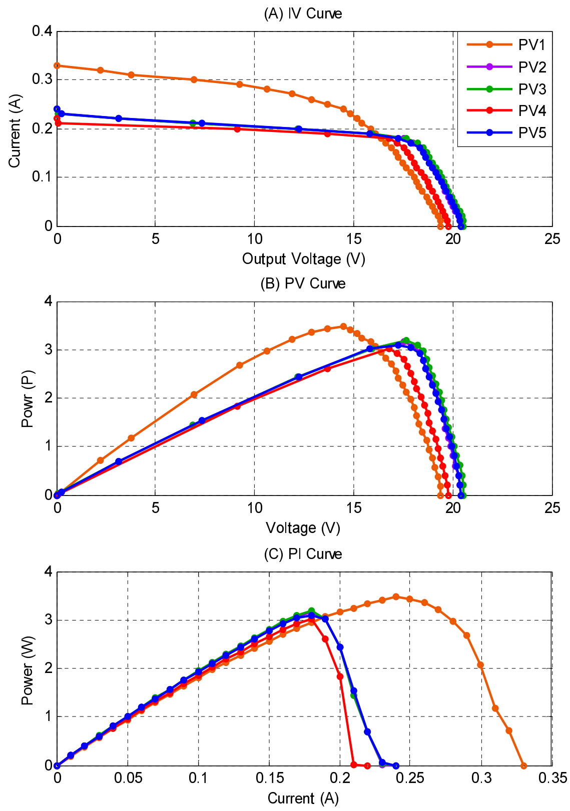

Fig. 21: Experimentally measured characteristic curves for 5 PV modules: (A) I-V Curves; (B) P-V Curves ;(C) P-I Curves.

In the Fig. 21, the experimentally measured characteristic curves of the five PV modules are presented. The measured characteristics among the five modules show big difference especially the orange curve (PV1), which has higher short circuit current and lower open circuit voltage compared with other four modules. Especially the measured purple, green and blue curves are almost overlapping, which means that the manufacture tolerance among the three modules (PV2, PV3 and PV5) is relatively small. Thus, these modules are used in the following experiments to analyze the effects of partial shading.

5.3. Characteristics under Shading Conditions

Different shading patterns are analyzed. Shading pattern A, corresponding to the cloud shading condition, is equivalent to the decreased light intensity condition. PV3 is used to and the change of light intensity is implemented by using different lamps: two $800W$ big lamps (BL) are used to represent no shading condition, several $100W$ small lamps (SL) are used for reduced light intensity under shading conditions. For instance, as shown in Fig. 22, the blue curve shows the curve of PV module without shading effect and '2BL' indicates that two $800W$ big lamps (BL) are used. Similarly, the red line shows the curve of PV module under a decreased light intensity and '1BL+4SL' represents one $800W$ big lamps (BL) and four $100W$ small lamps (SL) are used. With the decrease of the light intensity, both the measured I_{SC} and open circuit voltage V_{OC} are reduced, while the reduction in I_{SC} is significant. In the test, further remove one $100W$ small lamp represents a severer shading condition. The lowest light intensity condition is implemented with only one $100W$ small lamp. As illustrated in Fig. 10, the experimental curves show similar changing tendencies with the simulation results.

The experimental results for the shading pattern C is shown in Fig. 23, where the red curves shows the characteristics of the PV module with one sub-module shaded. By comparing with the simulation result shown in Fig. 12, the measured curves are fit with the simulation results. Caused by the shading pattern C, both I_{SC} and V_{OC} are decreased, especially the maximum output power decreases significantly. As illustrated in Fig. 12, when the shading pattern C occurs, the knee point of the I-V curves move close to the zero voltage side.

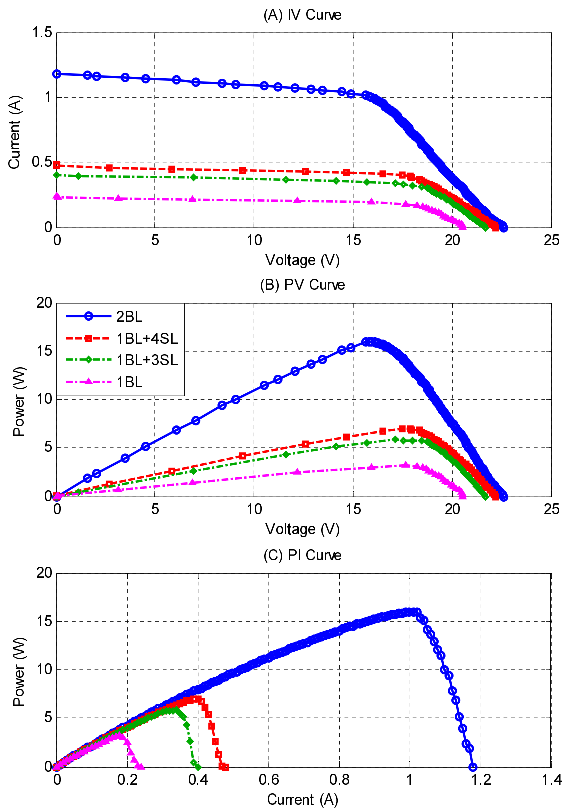

Fig. 22: Experimental curves of one module under shading pattern A: (A) I-V Curves; (B) P-V Curves ;(C) P-I Curves (BL: one $800W$ big lamps used in the experiment; SL: one $100W$ big lamps used in the experiment.

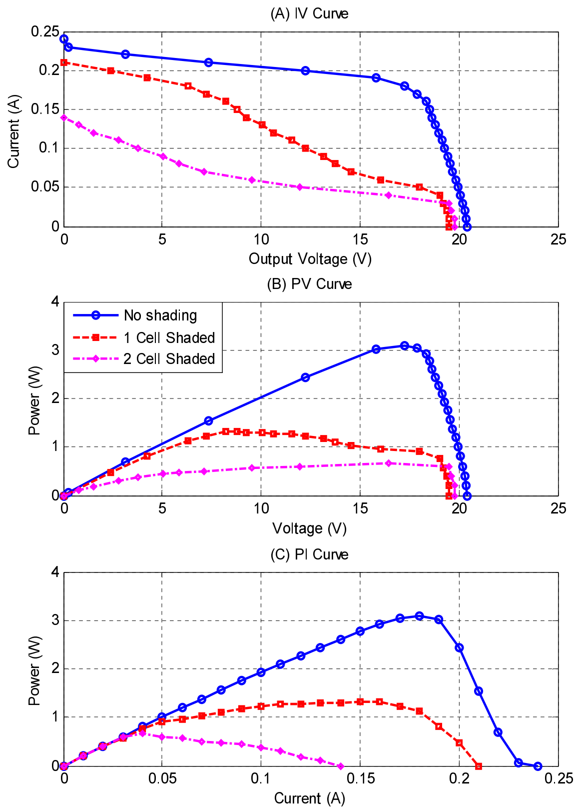

Fig. 23: Experimental curves of one module in shading condition C: (A) I-V Curves; (B) P-V Curves; (C) P-I Curves.

5.4. Converter Efficiency Test

Fig. 24 shows the measured efficiency of the sub-module based synchronous buck convert with respect to the output voltage. It shows that the designed SBC has very high efficiency especially for low output current conditions. For the same input voltage and output voltage, the efficiency decreases with the increase of the output current due to the increased power losses. In the efficiency calculation, only the conduction loss and switching loss are considered since the control loss can be neglected. The experiment results verified that the conduction loss and switching loss increase with the output current when the input and output voltage are fixed. The measured highest efficiency is 0.9873 when $I_{out} = 1A$ and $V_{in} = 10V$. When the input voltage is $12V$, the highest measured highest efficiency is 0.9895.

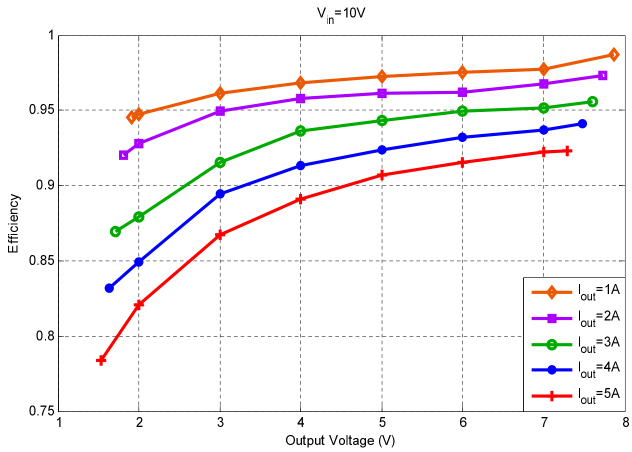

Fig. 24: Efficiency measurement for the synchronous buck converter under "$V_{in} = 10V$".

5.5. Experimental Result with the Proposed Sub-Module DMPPT

The output power with the proposed method is experimentally evaluated. Fig. 24 shows the experimental results comparison, where the aquamarine blue line ('PV3-1BL3SL') indicates the measured P-I character curve of the PV3 when module PV3 is exposed to one $800W$ big lamp and three $100W$ small lamps. The measured P-I curve of the PV2 is shown as the blue line, where PV2 is exposed to the highest intensity since two $800W$ big lamps are used. The purple line, symbolled as 'PV-s-sum' shows the mathematical power sum of PV2 and PV3. In order to emulate a PV module with two sub-modules series connected, sub-module PV2 and PV3 are series connected and their irradiations are set the same as previous experiments. The gray line, symbolled as 'PV-s-NoDiode', shows the P-I curve when no bypass diodes are parallel-connected with the PV sub-modules. It indicates that the short circuit current is significantly limited by the shaded sub-module PV3 since it is exposed to a lower intensity light. If bypass diodes are parallel-connected, the output current range is increased. However, the maximum output module current is still limited by the shaded sub-module PV3 by comparing curves 'PV-s-NoDiode' and 'PV2-2BL'. Furthermore, the gray curve 'PV-s-NoDiode' shows two maximum power points. Conventional MPPT algorithms will be lost around the local MPPT and a more complicated research algorithm is necessary to locate the global MPPT. In Fig. 24, the global maximum power of the green line is less than the maximum power of PV2 by comparing curves 'PV-s-Diode' and 'PV2-2BL'. Therefore, even the global MPP can be tracked, the maximum power by using the complicated algorithm is still reduced by the activation of bypass diodes. Replace the bypass diodes by the SBC based DC optimizer with sub-module DMPPT control, the experimental tests are made by recording the output power at different output current. As illustrated by the red curve of Fig. 24, the measured maximum power $15.44W$ when the output current is larger than $0.76A$. With the bypass diode, the measured global maximum power of the PV module with two sub-modules series connected is $12.10475W$ when the output current is $0.35A$. Then, the efficiency improvement by applying sub-module DMPPT can be calculated as 27.55%.

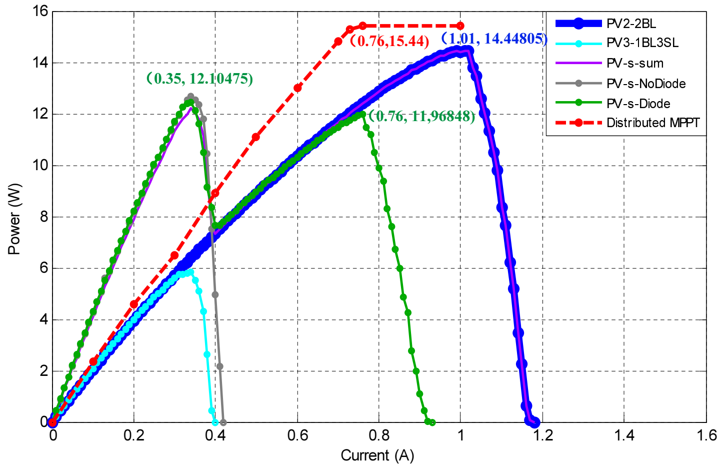

Fig. 25: Experimental results comparison.

6. Conclusion

In a PV power system, mismatch or partial shading issues for different level PV elements such as cells, sub-modules and modules have significant affects on the total power yield, lifetime, and reliability of a practical PV system. In this paper, a sub-module series-connected DC optimizer PV structure with the distributed maximum power point tracking (DMPPT) control is presented with aim to achieving optimal output power of the PV module even when mismatch conditions occur. Furthermore, in order to minimize the prototype size, reduce the system cost and improve efficiency, a two-switch synchronous buck converter (SBC) is implemented for each PV sub-module. By using 250kHz high switch frequency, the size of the SBC converter is minimized as small as a coin and can be directly mounted in the junction box of a solar module. Furthermore, higher conversion efficiency is achieved for a wide operating range compared with other topologies. A two-step perturb & observe based sub-module DMPPT algorithm is adopted. Specifically, a coarse tracking is firstly implemented with large step size in order to locate the operating point quickly. Then, the second stage is implemented with a small step size in order to minimize the static oscillations. In the proposed sub-module DMPPT algorithm, only the output voltage is required to sample, which removes the expensive current sensor and simplifies the practial control implementation. The experimental measured SBC highest efficiency is 98.7%. Furthermore, with the proposed sub-module DMPPT algorithm, a average 27.55% output power improvement is achieved through experimental test comparison.

7. Acknowledgement

This work was supported by the Research development fund of XJTLU (RDF-14-02-03), the State Key Laboratory of Alternate Electrical Power System with Renewable Energy Sources (LAPS15014), the National Nature Science Foundation of China (51407145) and the State Key Laboratory of Electrical Insulation and Power Equipment (EIPE15203).

8. Reference

[1] M. Dez-Mediavilla, M. Dieste-Velasco, M. Rodrguez-Amigo, T. Garca-Caldern, C. Alonso-Tristn, Performance of grid-tied pv facilities based on real data in spain: Central inverter versus string system, Energy Convers Manage 86 (2014) 1128–1133.

[2] Y. Du, D. D. C. Lu, G. James, D. J. Cornforth, Modeling and analysis of current harmonic distortion from grid connected pv inverters under different operating conditions, Sol. Energy 94 (2013) 182–194.

[3] S. H. Lee, S. G. Song, S. J. Park, C. J. Moon, M. H. Lee, Grid-connected photovoltaic system using current-source inverter, Sol. Energy 82 (5) (2008) 411–419.

[4] B. N. Alajmi, K. H. Ahmed, G. P. Adam, B. W. Williams, Single-phase single-stage transformer less grid-connected pv system, IEEE Trans. Power Electron. 28 (6) (2013) 2664–2676.

[5] B. Subudhi, R. Pradhan, A comparative study on maximum power point tracking techniques for photovoltaic power systems, IEEE Trans. Sustain. Energy 4 (1) (2013) 89–98.

[6] M. A. Elgendy, B. Zahawi, D. Atkinson, Operating characteristics of the p amp;o algorithm at high perturbation frequencies for standalone pv systems, IEEE Trans. Energy Convers. 30 (1) (2015) 189–198.

[7] A. Safari, S. Mekhilef, Simulation and hardware implementation of incremental conductance mppt with direct control method using cuk converter, IEEE Trans. Ind. Electron 58 (4) (2011) 1154–1161.

[8] M. A. Elgendy, B. Zahawi, D. J. Atkinson, Assessment of the incremental conductance maximum power point tracking algorithm, IEEE Trans. Sustain. Energy 4 (1) (2013) 108–117.

[9] Y. S. B. T. L. Kottas, A. D. Karlis, New maximum power point tracker for pv arrays using fuzzy controller in close cooperation with fuzzy cognitive networks, IEEE Trans. Energy Convers. 21 (3) (2006) 793803. doi:10.1109/TIE.2012.2198036.

[10] T. Radjai, L. Rahmani, S. Mekhilef, J. P. Gaubert, Implementation of a modified incremental conductance mppt algorithm with direct control based on a fuzzy duty cycle change estimator using dspace, Sol. Energy 110 (2014) 325–337.

[11] A. Chaouachi, R. M. Kamel, K. Nagasaka, A novel multi-model neuro-fuzzy-based mppt for three-phase grid-connected photovoltaic system, Sol. Energy 84 (12) (2010) 2219–2229.

[12] R. Rachchh, M. Kumar, B. Tripathi, Solar photovoltaic system design optimization by shading analysis to maximize energy generation from limited urban area, Energy Convers Manage 115 (2016) 244–252.

[13] M. Balato, M. Vitelli, Optimization of distributed maximum power point tracking pv applications: The scan of the power vs. voltage input characteristic of the inverter, Int. J. Electr. Power Energy Syst. 60 (2014) 334–346.

[14] T. A. B. N. M. A. . L. V. Pavan, A. M., The effect of manufacturing mismatch on energy production for large-scale photovoltaic plants, Sol. Energy 117 (2015) 282–289.

[15] K. Tsang, W. Chan, Maximum power point tracking for pv systems under partial shading conditions using current sweeping, Energy Convers Manage 93 (2015) 249–258.

[16] N. Bizon, Global extremum seeking control of the power generated by a photovoltaic array under partially shaded conditions, Energy Convers Manage 109 (2016) 71–85.

[17] P. Sharma, V. Agarwal, Exact maximum power point tracking of grid-connected partially shaded pv source using current compensation concept, IEEE Trans. Power Electron. 29 (9) (2014) 4684–4692.

[18] S. Silvestre, A. Boronat, A. Chouder, Study of bypass diodes configuration on pv modules, Appl. Energy 86 (9) (2009) 1632–1640.

[19] J. Solrzano, M. Egido, Automatic fault diagnosis in pv systems with distributed mppt, Energy Convers Manage 76 (2013) 925–934.

[20] M. Z. Ramli, Z. Salam, A simple energy recovery scheme to harvest the energy from shaded photovoltaic modules during partial shading, IEEE Trans. Power Electron. 29 (12) (2014) 6458 – 6471.

[21] M. Adly, A. H. Besheer, An optimized fuzzy maximum power point tracker for stand alone photovoltaic systems: Ant colony approach, IEEE Conf. on Ind. Electron. Appl. (2012) 113–119.

[22] K. Ishaque, Z. Salam, A deterministic particle swarm optimization maximum power point tracker for photovoltaic system under partial shading condition, IEEE Trans. Ind. Electron 60 (8) (2013) 31953206.

[23] A. K. Abdelsalam, A. M. Massoud, S. Ahmed, P. Enjeti, High performance adaptive perturb and observe mppt technique for photovoltaic-based microgrids, IEEE Trans. Power Electron. 26 (4) (2011) 10101021.

[24] N. T. Luat, L. Kay-Soon, A global maximum power point tracking scheme employing direct search algorithm for photovoltaic systems, IEEE Trans. Ind. Electron 57 (10) (2010) 34563467.

[25] G. R. Walker, P. C. Sernia, Cascaded dc-dc converter connection of photovoltaic modules, IEEE Trans. Power Electron. 19 (4) (2004) 1130 – 1139.

[26] W. J. Cha, Y. W. Cho, J. M. Kwon, B. H. Kwon, Highly efficient microinverter with soft-switching step-up converter and single-switch-modulation inverter, IEEE Trans. Ind. Electron 62 (6) (2015) 3516–3523.

[27] R. C. Pilawa-Podgurski, D. J. Perreault, Submodule integrated distributed maximum power point tracking for solar photovoltaic applications, IEEE Trans. Power Electron. 28 (6) (2013) 2957–2967.

[28] R. Carbone, Pv plants with distributed mppt founded on batteries, Sol. Energy 122 (2015) 910–923.

[29] S. M. Chen, T. J. Liang, K. R. Hu, Design, analysis, and implementation of solar power optimizer for dc distribution system, IEEE Trans. Power Electron. 28 (4) (2013) 1764–1772.

[30] T. Shimizu, M. Hirakata, T. Kamezawa, H. Watanabe, Generation control circuit for photovoltaic modules, IEEE Trans. Power Electron. 16 (3) (2001) 293–300.

[31] A. Urtasun, D. D. C. Lu, Control of a single-switch two-input buck converter for mppt of two pv strings, IEEE Trans. Ind. Electron 62 (11) (2015) 7051–7060.

[32] A. Urtasun, P. Sanchis, L. Marroyo, Adaptive voltage control of the dc/dc boost stage in pv converters with small input capacitor, IEEE Trans. Power Electron. 28 (11) (2013) 5038–5048.

[33] Z. Zhao, M. Xu, Q. Chen, J. S. Lai, Y. Cho, Derivation, analysis, and implementation of a boostbuck converter-based high-efficiency pv inverter, IEEE Trans. Power Electron. 27 (3) (2012) 1304–1313.

[34] G. Petrone, G. Spagnuolo, M. Vitelli, Modeling and control of pv charger system with sepic converter, IEEE Trans. Ind. Electron 56 (11) (2009) 4344–4353.

[35] R. Kumar, B. Singh, Bldc motor driven solar pv array fed water pumping system employing zeta converter, IEEE Trans. Ind. Appl. 99 (2016) 1–1.